Investigation of indium distribution in InGaAs/GaAs quantum dot stacks using high-resolution x-ray diffraction and Raman scattering

Yu. I. Mazur,[a] Zh. M. Wang, and G. J. Salamo
Department of Physics, University of Arkansas, Fayetteville, Arkansas 72701

V. V. Strelchuk, V. P. Kladko, V. F. Machulin, and M. Ya. Valakh
Lashkaryov Institute of Semiconductor Physics, NAS of Ukraine, Prospect Nauky 45, 03028 Kyiv, Ukraine

M. O. Manasreh
Department of Electrical Engineering, 3127 Bell Engineering Center, University of Arkansas, Fayetteville, Arkansas 72701

(Received 16 June 2005; accepted 2 December 2005; published online 24 January 2006)

Using high-resolution x-ray diffraction (HRXRD), Raman scattering, photoluminescence, and atomic-force microcopy, we investigated $In_xGa_{1-x}As/GaAs$ quantum dot (QD) stacks grown by molecular-beam epitaxy with nominal In contents of 0.30 and 0.35. The analysis of x-ray-diffraction rocking curves using symmetrical (004), asymmetrical (113), and quasiforbidden (002) reflections within the framework of dynamical theory allowed us to determine the average values of strains parallel and perpendicular to the growth direction. We also measured nonuniform In profiles in the $In_xGa_{1-x}As$ layers along the growth direction. This observation confirms the important role of surface segregation of In atoms and interdiffusion of Ga atoms from GaAs layers in the formation of $In_xGa_{1-x}As$ QDs. Both HRXRD and Raman scattering in $In_xGa_{1-x}As/GaAs$-stacked QD structures demonstrate that the InGaAs inserts in these structures can be modeled effectively as sublayers with two different compositions: sufficiently thick $In_xGa_{1-x}As$ sublayer with the In concentration lower than the nominal one, which includes the thin layer of InGaAs islands with the In concentration much higher than the nominal one. © *2006 American Institute of Physics*. [DOI: 10.1063/1.2163009]

I. INTRODUCTION

The In(Ga)As/GaAs material system has been the focus of research interests because it can result in self-assembled confined structures, such as quantum dots during epitaxial growth.[1] Quantum dots (QDs) offer the potential for application as electronic and optoelectronic devices, such as lasers,[2] optical memories,[3] and infrared photodetectors.[4]

QD formation in mismatched heteroepitaxial systems such as $In_xGa_{1-x}As/GaAs$ is generally considered to take place when the reduction of the elastic strain in the deposited two-dimensional (2D) epitaxial layer is larger than the increase in surface energy associated with the three-dimensional (3D) QD formation. However, the process of QD formation is much more complex than the simple picture based on the principle of free-energy minimization would imply. For example, intermixing and segregation of In atoms are intertwined with energy considerations and play a significant role in determining the strain distribution, the critical thickness $t_{3D}(x)$ for the 2D to 3D transition,[5] the surface density, and the size and shape[6–8] of the QDs. Investigations of intermixing for InAs QDs grown on GaAs (001) substrates ($420\ ^\circ C < T_s < 500\ ^\circ C$) using transmission electron microscopy,[9] scanning tunneling microscopy,[10] and x-ray diffraction[11,12] show a substantial mass transfer from the wetting layer and the GaAs substrate to the QDs. In fact, it has been shown that the Ga content in the InAs QDs can reach 50%–60%. This can be understood by the segregation of In atoms during the growth of InAs, which is accompanied by the generation of vacancies. The vacancies are in turn filled by migrating Ga atoms from the GaAs buffer layer.[9] Of course, the whole process is intimately connected to the strain distribution.

Indium-atom segregation also explains the formation of islands with increased (up to ~60%) In concentration in the core of QDs during the growth of $In_{0.25}Ga_{0.75}As$ on a GaAs (001) substrate ($T_s = 540\ ^\circ C$).[13] While In segregation and In–Ga interdiffusion and their corresponding relationship with strain, definitely, play a complicated role in the formation of InGaAs QD structures, the mechanism for intermixing in InAs QDs is not certain and additional quantitative studies on the indium and gallium distributions are needed to understand and control QD formation.

In this paper we report our investigations of the indium (In) distribution in self-assembled, multiple layered, $In_xGa_{1-x}As/GaAs$ QD structures. We report on high-resolution x-ray-diffraction (HRXRD) investigations that give evidence for a nonmonotonic In content in the InGaAs layer. In particular, we show that the In content can be modeled as a bimodal distribution in a InGaAs layer composed of a In-poor 2D layer with $x_1 < x_{nom}$ and an In-riched layer with $x_2 > x_{nom}$. In addition to the HRXRD data we also report Raman data, which further support the existence of a bimodal In distribution.

[a]Electronic mail: ymazur@mail.uark.edu

II. EXPERIMENTAL APPROACH

The growth of $In_xGa_{1-x}As/GaAs$ QD multilayers was carried out in a commercial solid-source Riber-32 molecular-beam epitaxy (MBE) system equipped with a reflection high-energy electron-diffraction (RHEED) system and a highly accurate (±2 °C) optical transmission thermometry system for substrate temperature determination and reliability. Epitaxial-ready semiinsulating GaAs (001) substrates were loaded into the MBE growth chamber. After the surface oxide layer was removed, a 0.5−μm-thick GaAs buffer layer was grown at 580 °C with a growth rate of 1.0 ML/s. During the growth of all the samples, the As beam equivalent pressure from a valve-controlled cell was kept constant at 1×10^{-5} Torr. The substrate temperature was reduced to 520 °C for the growth of two complete sets of samples having a structure of eight periods of $In_xGa_{1-x}As$ (14 ML)/GaAs (70 ML). While the nominal layer thickness of these samples was constant, the nominal In compositions were 0.30 and 0.35 for the first set and the second set of samples, respectively. The In composition variation for different sample sets was achieved by performing the $In_xGa_{1-x}As$ growth with the In flux corresponding to a 0.2 ML/s growth rate and the Ga flux adjusted by changing the Ga source temperature. Surface evolution during $In_xGa_{1-x}As$ growth was monitored by the RHEED. The 3D growth mode transition was observed using the RHEED pattern transition from streaky to spotty. This transition occurred after an $In_xGa_{1-x}As$ deposition of 10.7 and 7.4 ML for samples with In contents of 0.3 and 0.35, respectively. Structural information was obtained from atomic force microscopy (AFM) (in contact mode) of the last but uncapped QD layer.

The samples were then analyzed using HRXRD to investigate both the In and strain distributions. In the experiments reported here, measurements of x-ray rocking curves on the symmetrical (004), asymmetrical (113), and quasiforbidden (002) reflections were carried out using a double-crystal diffractometer [crystal-monochromator GaAs 001, Cu Kα1 emission (λ=1.5406 A), and fourth reflection order]. Reciprocal-space maps (RSMs) around the (004) and (224) reciprocal-lattice points have been recorded using a diffractometer in triple axis configuration (Philips MRD X-Pert). Samples were scanned in the vicinity of the exact Bragg position and the thickness of the layers in the multilayer QD structures were determined using reflection oscillations in the Bragg diffraction signal. Measurements were carried out in the discrete angle mode with a step angle of 2 arc sec. A comparison of the experimental and calculated rocking curves was carried out using the χ^2 method that made it possible to estimate the average values of the parameters of interest as well as their uncertainty.

The same samples were then analyzed using Raman scattering to investigate the In content by studying the corresponding phonon spectrum. The Raman spectra were investigated using a cw Nd-YAG (yttrium aluminum garnet) laser oscillating at 1.064 μm and a Bomem Raman Fourier-transform interferometer in the regular backscattering geometry. All Raman measurements were performed at room temperature.

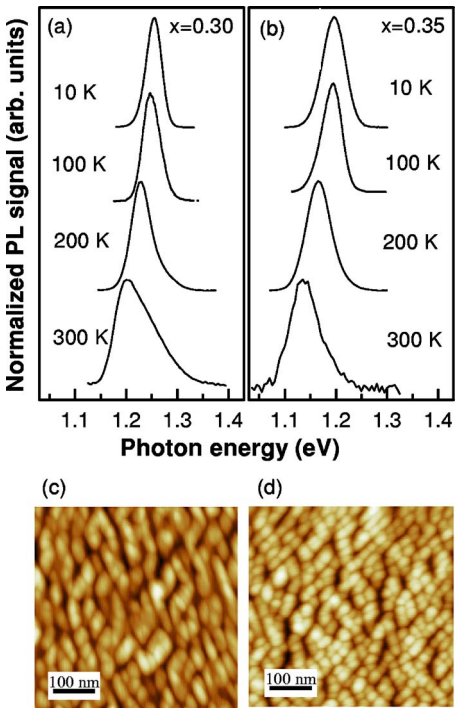

FIG. 1. (Color online) [(a) and (b)] Normalized PL spectra of the $In_xGa_{1-x}As/GaAs$ structures (x=0.30 and x=0.35, respectively); [(c) and (d)] AFM images of the grown QDs upon $In_xGa_{1-x}As$ layers with a nominal In concentration of 0.30 and 0.35, respectively.

In addition to the HRXRD and Raman-scattering data, we also investigated photoluminescence (PL) for each of our samples in order to identify their energy-level structure. The PL measurements were made over the temperature range of 4.2–300 K using a liquid-nitrogen-cooled Ge-diode detector. The 488.0 nm line of an argon-ion laser was used for excitation and the spectra were recorded using a standard lock-in detection technique. The laser beam spot sizes on the samples in the PL measurements were approximately 100 μm.

III. EXPERIMENTAL OBSERVATIONS AND DISCUSSIONS

A. Photoluminescence, atomic force microscopy, and x-ray reciprocal-space mapping

The energy-level structure and the quality and geometry of the QDs were monitored using PL and AFM, respectively. The PL spectra of the samples as a function of temperature, with nominal In compositions of x=0.30 and x=0.35, are shown in Figs. 1(a) and 1(b), respectively. The spectrum for each sample consists of a single band due to emission from $In_xGa_{1-x}As$ QDs. Under weak excitation, above the GaAs barrier band gap, this PL band at 10 K is centered at 1.254 and 1.197 eV with a full width at half maximum (FWHM) of 37 and 50 meV for the samples with x=0.30 and x=0.35, respectively. Each peak can be fitted well by a single Gaussian profile, suggesting reasonable homogeneity of the QDs around one dominant size. With increasing temperature, the

QD emission band was observed to shift toward lower energy, almost maintaining its shape until ≈200 K. At higher temperatures ($T>80$ K), the overall PL integrated intensity is observed to decrease most likely as a consequence of exciton dissociation resulting in electron-hole pairs escaping from the QDs.

AFM images of the uncapped $In_xGa_{1-x}As$ QDs are shown in Figs. 1(c) and 1(d). The major and minor axes of the elliptical $In_xGa_{1-x}As$ dots are oriented along the $[\bar{1}10]$ and [110] directions, respectively. Furthermore, the average major and minor axes of elliptical dots are observed to decrease from 42 to 35 nm and from 22 to 15 nm, respectively, with the increase of x from 0.30 to 0.35 [Figs. 1(c) and 1(d)]. When x grows from 0.30 up to 0.35, the decrease in the average dot size is associated with a dramatic increase in QD density [Fig. 1(d)]. The corresponding area density of the QDs is as high as 95%, and the dots are nearly in contact with each other. Another difference is that the QD's distribution (sizes and interdot spacing) at $x=0.35$ is more uniform as compared to that of $x=0.30$. We did not see evidence, in either sample, of dot coalescence or very large islands with edge dislocations, which can occur in the case of InAs QDs. Based on previous reports,[6] this unique behavior can be accounted for by the existence of an inhomogeneous distribution of In and Ga in the $In_xGa_{1-x}As$ arising from segregation of In to the top of the QDs. This segregation dramatically lowers the nucleation barrier for QDs and can prevent dot coalescence for $In_xGa_{1-x}As$ QDs.

Figures 2(a) and 2(b) show the RSMs recorded close to the (004) and the (224) Bragg reflection by the substrate for the sample with $x=0.30$. Using this RSM of diffracted intensity, one can see the system of spatial-ordered peaks both along the growth direction q_z [along the diffraction vector for the (004)] and in the interface plane (in q_x direction), which indicates formation of the long-range order in the scattering center arrangement in the direction of growth.[14] The distance between superstructural sharp peaks along the diffraction vector at $q_x=0$ corresponds to the superlattice vertical period ($\Lambda^{SL}=22.9\pm0.2$ nm), and in the lateral directions—to the QD lateral period ($\Lambda^{QD}=80.0\pm0.2$ nm).

Shown in Fig. 2(c) is the dependence of the diffracted radiation intensity on the diffraction angle (Θ_{Br}) in the ($\omega-2\Theta$)-scanning technique for the sample with $x=0.30$. The curve a was obtained using the three-crystal experimental geometry, which corresponds to the RSM section along the line of coherent superlattice satellites [(004) reflection, Fig. 2(a)]. In this geometry, scattered radiation falls onto a detector after an analyzer, which results in a considerable decrease of the diffuse component of the x-ray beam diffracted from QD (it is practically suppressed). The curve b was obtained using the double-crystal diffraction geometry with a broad slit in front of the detector, and, effectively, is a superposition of coherent and diffuse scattering components integrated over the Ewald sphere. It can be seen that except for (In,Ga)As–GaAs satellites of the multilayer structure, which are responsible for the superlattice vertical period, the rocking curve shows diffuse peaks (satellites) caused by the

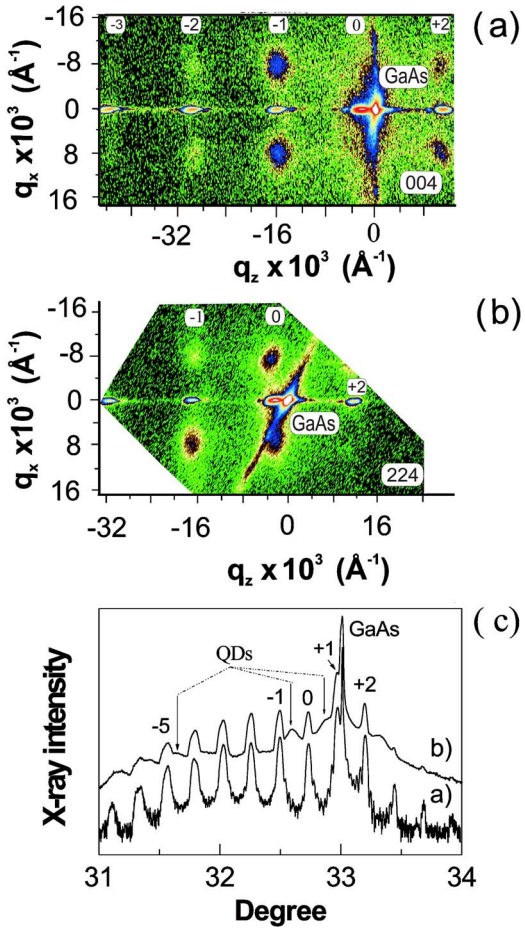

FIG. 2. (Color online) [(a) and (b)] Reciprocal space maps around (004) and (224) GaAs Bragg reflections for the sample with $x=0.30$. (c) $\omega-2\Theta$ line scans for (004) reflection taken in the three-crystal (curve a) and double-crystal (curve b) geometries.

QDs. Since these scans were more informative than the three-crystal scans; the double-crystal geometry was used in the experiments (Sec. III B).

B. High-resolution x-ray diffraction

The In distribution in our samples was examined using HRXRD. Measured spectra of x-ray diffraction were modeled as a multilayered quantum-well structure. Each of the layers was represented as a system of uniform sublayers (lamellas).[15] The calculations of the rocking curves were carried out using the dynamic theory formula of x-ray scattering that can be reduced to recurrent relations connecting the amplitude of $R_{h,N}$ (Nth-layer reflection) with the amplitudes of the $R_{h,1}$ (reflection) and the $R_{0,1}$ (transmission) of the upper layer and the amplitudes of the $(N-1)$ layer,[16]

$$R_{h,N}=[R_{h,1}+R_{h,N-1}(R_{0,1}R_{0,1}-R_{h,1}R_{h,1})]\times(1-R_{h,N-1}R_{h,1})^{-1}. \quad (1)$$

Each of the layers is characterized by a thickness t_j, lattice parameter a_j, and the static Debye-Waller factor that is associated with shifts of atoms from their regular positions.

In Fig. 3 we plot the high-resolution double-crystal rocking curves ($\omega-2\Theta$ scans) for the symmetrical (004) Bragg reflection of a sample (solid lines) together with a simulation

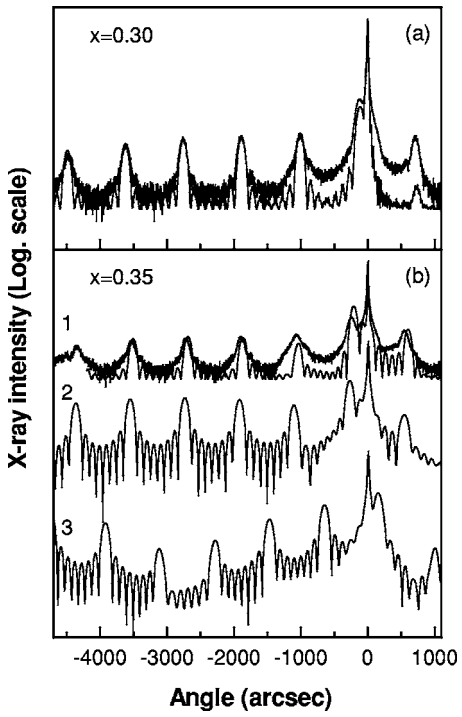

FIG. 3. (004) Bragg reflection ω-2Θ scan of the $In_xGa_{1-x}As/GaAs$ multilayers structures for nominal In composition of (a) 0.30 and (b) 0.35 (solid lines), respectively, together with their simulated spectra (gray lines). The calculated curves in (b) are curve 3—single-layer model with strains preset by the technological thicknesses, curve 2—two-layer model using a thicknesses of 1.6 and 3.5 nm with In contents of 55% and 23%, respectively, and curve 1—two-layer model with parameters presented in Table I.

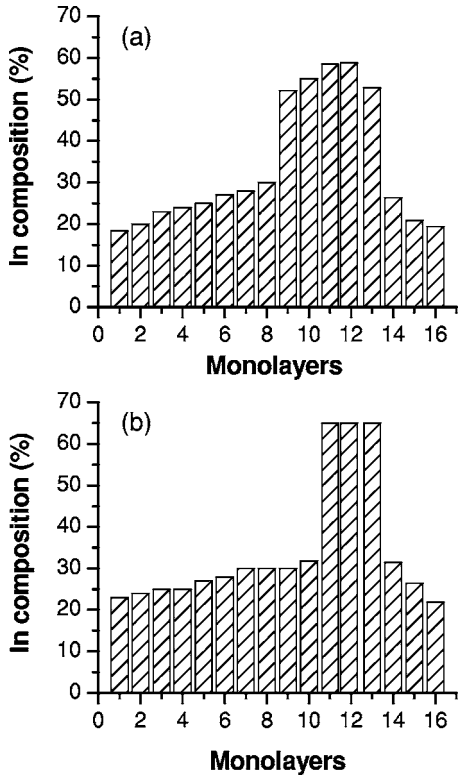

FIG. 4. Indium composition profiles for multilayer $In_xGa_{1-x}As/GaAs$ structures obtained by modeling symmetrical (004) reflection within 16-layer model for the samples with the nominal In concentration $x=0.35$: (a) with parameters close to simulation curve 2 for (004) reflection in Fig. 3(b) and (b) curve 1 in Fig. 3(b).

using dynamical diffraction theory (gray lines) for $x=0.30$ and $x=0.35$, respectively. The theoretical curve neglects the formation of InGaAs islands and considers only 2D InGaAs layers. Along with the substrate peak and the main peak caused by the averaged lattice structure (zeroth-order satellite), one can observe the complex interference structure at the rocking curve tails, the so-called "satellite structure."[17] On each curve (Fig. 3), satellite peaks, up to seven orders, are observed, which is evidence for the sharp interfaces of the multilayered structure and for a well-defined periodicity. The distance between the observed satellite peaks is related to the multilayer periodicity of the structure. It is important to note that the symmetrical (004) reflection is only sensitive to the lattice strain perpendicular to the layers.

Using the relations in Ref. 16, we carried out calculations of the rocking curve spectra for each of the structures. The parameters of the structures were used as the initial conditions for fitting the theoretical HRXRD spectra to the experimental data. Modeling the HRXRD spectra using a single-layer model with known parameters did not compare well with the experimental and simulation reflection curves [curve 3, Fig. 3(b)]. During the fitting procedure we began by using a 14-layer model (according to the nominal number of InGaAs monolayers). Figures 4(a) and 4(b) show two possible distribution profiles of In in the $In_xGa_{1-x}As$ layers in the growth direction for the sample with $x_{nominal}=0.35$ obtained as a result of modeling with parameters close to the simulated curves 2 and 1 in Fig. 3(b), respectively. The obtained fitting results have shown that for the investigated samples a good approximation can be obtain only by modeling the InGaAs region using two sublayers of different thicknesses and with strongly different component compositions, e.g., a thick sublayer with a low In concentration followed by (moving along the growth direction) a thin sublayer with a high In concentration. Curve 2 in Fig. 3(b) corresponds to the modeling by the two-layer model using thicknesses of 1.6 and 3.5 nm with In compositions of 55% and 23%, respectively. The best agreement of the theoretical and experimental curves was obtained using a two-layer model with parameters presented in Table I [curve 1 in Fig. 3(b)]. A 16 ML total thickness instead of the nominal 14 ML of InGaAs layer was needed for the best modeling.

As a result, we obtained an average In concentration within the $In_xGa_{1-x}As$ sublayers, as well as the variation of the lattice parameter perpendicular to the layer plane. These results are summarized in Table I. For example, Table I shows the value of the deformation parameter $\langle \varepsilon_0 \rangle$ averaged over the period of the multilayer structure along the growth direction. The deformation was calculated using the formula,

$$\langle \varepsilon_0 \rangle = \frac{\varepsilon_1 t_1 + \varepsilon_2 t_2}{t_1 + t_2}, \tag{2}$$

where ε_1, t_1 and ε_2, t_2 are the averaged values of deformation and thickness of $In_xGa_{1-x}As$ and GaAs layers, respectively. Also shown in Table I, the mean value of the deformation in the multilayered structure $\langle \varepsilon_{S0} \rangle$ was obtained using the value of the measured angle position for the zeroth satellite.

TABLE I. Parameters of multilayer $In_xGa_{1-x}As$ structures obtained from modeling (004) x-ray-diffraction rocking curves.

	Data obtained as a result of modeling								
					Deformation[a] in layers in the growth direction of the structure				
Nominal In composition in $In_xGa_{1-x}As/GaAs(x)$	In composition in $In_xGa_{1-x}As$ layers (x)	$In_xGa_{1-x}As$ quantum layer thickness (nm)	GaAs layer thickness (nm)	Multilayer structure period (nm)	$\varepsilon_1^{\perp}$ ($In_xGa_{1-x}As$)	$\varepsilon_2^{\perp}$ (GaAs)	$\Delta a/a$ in relaxed periods of the multilayer structure	$\langle\varepsilon_0\rangle$	$\langle\varepsilon_{S0}\rangle$
0.30	0.52 0.2	0.85 3.9	16.94	21.69	0.03 0.029	0.001 85	0.004 44	0.007 79	0.007 54
0.35	0.65 0.25	0.7 4.4	17.88	22.98	0.045 0.0322	0.000 75	0.004 53	0.008 34	0.007 99

[a]For the symmetric reflections of (004) and (002), deformation was calculated in the direction of the scattering vector, which in this case coincides with the growth direction.

It is seen from the figure [Fig. 4(b)] that the distribution profile of In in the $In_xGa_{1-x}As$ layers is asymmetrical, and the maximum In concentration is shifted in the direction of growth. Indium segregation in the $In_xGa_{1-x}As$ layer and Ga interdiffusion from the barrier layer into the $In_xGa_{1-x}As$ layer,[7,10] driven by a strain distribution resulting from the 2D to 3D transition, are likely to work together to explain the sublayer In redistributions.

From this viewpoint, such a simple two-layer model is rather crude and is in contradiction with the conventional Stranski-Krastanow model of 3D-island growths. But currently it is well known that the Stranski-Krastanow model gives only the main features for the self-organized mechanism of 2D-3D transformation in epitaxial growth of strained semiconducting systems, especially for mixed semiconductors (e.g., $In_xGa_{1-x}As$ in our case). There is a variety of complications, and among them—the influence of segregation and dramatic effect of interdiffusion, stimulated by nonuniform strain fields. As a result, in reality the transition from the 2D-layer growing mode to the 3D-island one can be realized through the islands of 2D type (platelets). The chemical composition of the platelets differs essentially from chemical compositions of 2D layer in which they are embedded and they fulfill the role of precursors in 3D-island growth. This type of the mechanism for 2D-3D transformation was theoretically analyzed by Priester and Lannoo.[18] From our viewpoint, the excellent experimental evidences of 2D-platelets precursors were given in the case of A^3B^5 nanostructures[19] as well as for A^2B^6 nanostructures.[20] Reference 21 also gives strong evidence for this precursor. The experimental data pictured in Refs. 18–21 give evidence that for the sufficiently large surface density of 2D platelets these may be approached as forming 2D inserts with elevated In content in $In_xGa_{1-x}As$-layer with lower In content (or elevated Cd content in $Cd_xZn_{1-x}Se$ layer).

These experiments point out that for a nominal thickness of $In_xGa_{1-x}As$ layers that is slightly above the 2D-3D transition a two-layer model with different In contents may be used as reasonable approximation within the restricted thickness limits. It seems rather probable that in our case such a situation was realized. Indeed, as seen from the AFM data [Figs. 1(c) and 1(d)] the nanoisland surface density is very high ($\sim$95%), and the nanoislands are in a close contact with each other. At the same time, the average height (h) of nanoislands is much less then their lateral size (l)($h/l \sim 1/30-1/40$). Therefore, they can be really considered as platelets. The fact that a total thickness of 16 ML of InGaAs was needed instead of the nominal 14 ML layer for the best modeling of experimental x-ray data is also consistent with our assumption. The fact that an extra thickness (as compared with the nominal one) of InGaAs (CdZnSe) layers was also noted in Refs. 19 and 20. However, when the nominal thickness of InGaAs layer in these multilayer structures increases and Stranski-Krastanow 3D islands of pyramidal shape are formed from 2D precursors the two-layer model will become crude.

It is of interest that the analysis of symmetrical reflections only allows one to obtain the strain perpendicular to the layer plane. In-plane strains on the other hand can be determined from an analysis of asymmetrical reflections. In Fig. 5 the experimental result for the asymmetrical (113) reflection in the geometry of grazing incidence is shown together with a simulation using nearly the same parameters (within experimental error of 3%–5%) used for the (004) reflection in Fig. 3. The results from fitting the experimental data for the (113) reflection are summarized in Table II. These results, taken together with the (004) reflection data, give further support for the bimodal distribution described above for the samples with $x=0.30$ and $x=0.35$.

Thus the experimental data obtained using (004) and (113) reflections, together with a theoretical model, enable us to draw the conclusion that the $In_xGa_{1-x}As$ layer can be effectively modeled as two sublayers: a 2D layer with a low In concentration and a layer with 3D islands possessing a greater In concentration.

Consistent with this conclusion is the result from the (002) reflection data (see Fig. 6), which shows one additional satellite (of the positive order "+1") at the side of the rocking curve. The intensity of this satellite peak unexpectedly exceeds that of the zeroth-order satellite. Our analysis of the intensity ratio of the first-order satellites to the zeroth-order satellite for the (002) reflection is in fact very sensitive to the

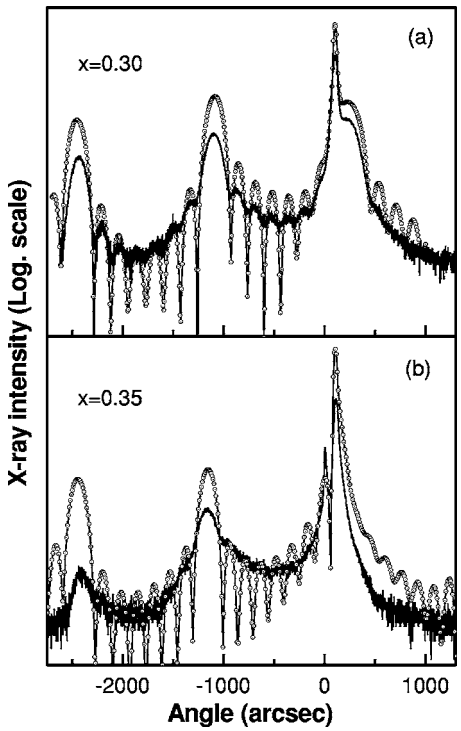

FIG. 5. Double rocking curves of the asymmetric (113) Bragg reflection together with simulation with the same parameter set as for the (004) reflection of multilayer $In_xGa_{1-x}As$ structures with nominal In concentrations of (a) 0.30 and (b) 0.35.

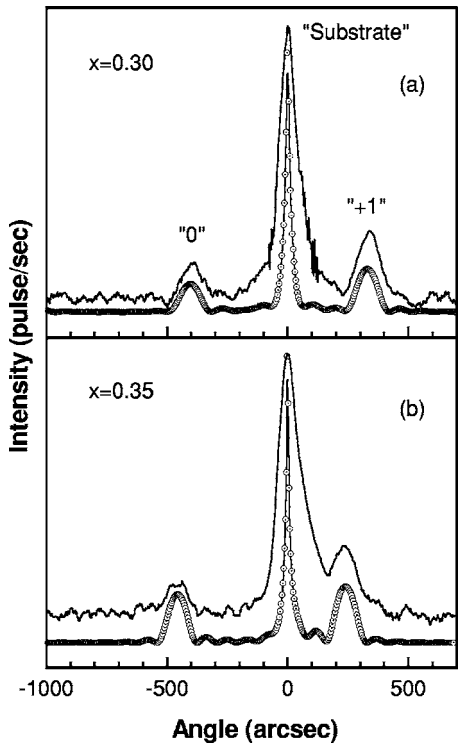

FIG. 6. Experimental (solid line) and its dynamical simulation (open circles) (002) diffraction rocking curves for multilayer $In_xGa_{1-x}As/GaAs$ structures with nominal In concentration of 0.30 (a) and 0.35 (b).

alloy composition. At certain values of composition ($x > 0.5$) this ratio (for the positive satellite) can substantially exceed 1. Therefore, contributions from the sublayer with a small In content and the GaAs layer play a small role [as a consequence of small values of (002) reflection structural factors in these compounds]. Consequently, the relationship between satellite intensities in the spectra of the (002) reflection is determined mainly by the contribution of the sublayer with the greater In content. At the same time, the satellite periodicity is not destroyed since it depends on the total thickness of the layer. The results of the simulation the (002) reflection using two-layer model that confirm the presence of sublayers with low and high concentrations of In are shown in Fig. 6 as well. In this case, the (002) reflection data are also consistent with a bimodal In distribution model.

TABLE II. Parameters of layer deformations in the interface plane obtained from the data of the asymmetrical (113) x-ray-diffraction rocking curves.

	Data obtained as a result modeling			
		Deformation[a] in the lateral direction of structure		
Nominal In composition in $In_xGa_{1-x}As$(x)	In composition in $In_xGa_{1-x}As$ layers (x)	ε_1^{II} ($In_xGa_{1-x}As$)	ε_2^{II} (GaAs)	Deformation in GaAs-cap layer
0.3	0.53	0.0385	0.0006	0.0050
	0.2	0.007		
0.35	0.65	0.017	0.0015	0.0008
	0.28	0.006		

[a]For the reflection of (113), deformation was calculated in the direction of the diffraction vector.

C. Raman scattering of $In_xGa_{1-x}As/GaAs$ multilayer structures

Given that the HRXRD data suggested that the $In_xGa_{1-x}As$ layers could be modeled by two sublayers having different In concentrations (i.e., bimodal In distribution), we looked to Raman spectroscopy to further check this conclusion. Figure 7 shows the Stokes and anti-Stokes Raman spectra for the two multilayered $In_xGa_{1-x}As/GaAs$ structures with In concentrations of 0.30 and 0.35 (curves 2 and 3), respectively. Curve 1 in Fig. 7 corresponds to the Raman spectrum from a reference GaAs/GaAs (100) structure grown under the same conditions as the $In_xGa_{1-x}As/GaAs$ structures. The thickness of the GaAs epilayer is equal to the total thickness of the barrier GaAs layers in the $In_xGa_{1-x}As/GaAs$ structures.

Since the Raman pump or excitation energy, $E_{exc} = 1.165$ eV (1.064 μm), is well below the direct gap of GaAs (1.429 eV at room temperature), Raman-scattering investigations of the GaAs layers (Fig. 7, curve 1) are nonresonant. The first-order Raman spectra for the sample with the GaAs epilayer show a strong line at 291.6 cm^{-1} corresponding to scattering by longitudinal-optical (LO) GaAs phonons [Figs. 7(a) and 7(b), curve 1]. There is also a weaker line at 266.3 cm^{-1} corresponding to scattering by transverse-optical (TO) GaAs phonons. The presence of the TO (GaAs) mode in the Raman spectra is possibly due to small deviations in the light propagation direction inside the sample from the crystallographic [001] direction. Most of the weak features in

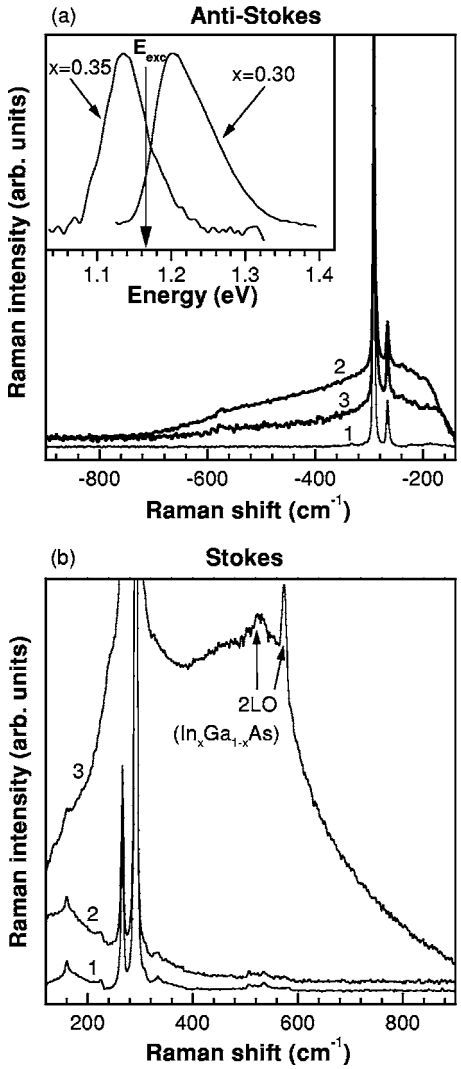

FIG. 7. (a) Anti-Stokes and (b) Stokes Raman spectra of GaAs epilayer (curve 1) and $In_xGa_{1-x}As/GaAs$ multilayer structures with nominal In concentrations of 0.30 and 0.35 (curves 2 and 3, respectively). Spectra are normalized to the intensity of LO (GaAs) line. Curve 1 is vertically shifted downwards for clarity ($E_{exc}=1.165$ eV and $T=300$ K). In the inset of (a), PL spectra of samples with $x=0.30$ and $x=0.35$ obtained under $E_{exc}=2.54$ eV and $T=300$ K are shown; the excitation energy for the Raman spectra is indicated by an arrow.

these spectra are attributed to second-order Raman scattering by GaAs phonons.[22] The peak positions of the LO modes and the intensity ratio $I(LO)/I(TO)$ for GaAs, for all the Stokes and anti-Stokes spectra (Fig. 7, curves 1, 2, and 3) discussed in this paper, do not change within our experimental accuracy, indicative of insignificant changes of the crystal structure quality and strain values in the GaAs structure.

Raman spectra become a bit more complicated when studying $In_xGa_{1-x}As/GaAs$ multilayered structures due to resonant excitation in the range of the $In_xGa_{1-x}As$ QD (nanoislands) emission band. We carried out theoretical estimations of the energy of the exciton ($e1-hh1$) transition ($T=300$ K) for two sublayers by approximating the layers as a quantum well. Under this approximation, the energy of the transition for the 2D $In_xGa_{1-x}As$ layer ($d=4$ nm, $x=0.25$) is equal to ≈ 1.18 eV while for the thin layer ($d=1$ nm, $x=0.65$) ≈ 1.11 eV. Thus, at an $E_{exc}=1.165$ eV, the excitation is near resonant for the 2D $In_xGa_{1-x}As$ layer (incoming resonance), as well as for the $In_xGa_{1-x}As$ layer with nanoislands (outgoing resonance).

As seen from the inset in Fig. 7, the excitation photon energy is from the low-energy side of the $In_xGa_{1-x}As$ nanoislands emission band ($E_{max}^{PL}-E_{exc}\approx 37$ meV) for $x=0.30$, while the excitation is from the high-energy side ($E_{exc}-E_{max}^{PL}\approx 30$ meV) for $x=0.35$. Therefore, the resonant effects are expected to play a role in the observed Raman spectra. For both samples, the deformation potential for scattering TO phonons is much weaker than the Fröhlich mechanism for scattering by LO phonons. Therefore, the spectra of resonant or near resonant Raman scattering are expected to be dominated by multiphonon scattering from the LO phonons. In addition, if the energy of the incident or scattered light is near the energy of the exciton transitions in the $In_xGa_{1-x}As$ layers (incoming and outgoing resonance conditions, respectively) the cross section for scattering in the $In_xGa_{1-x}As$ sublayers can be increased by several orders of magnitude. Of course, in this case, analyses of Raman spectra for $In_xGa_{1-x}As$ layers are further complicated by absorption, which results in a variable penetration depth of the excitation light. The situation is further complicated due to the different resonant properties of the Stokes and anti-Stokes-scattering processes.[23]

The resonant behaviors of the Stokes- and anti-Stokes-scattering components in our experiment are shown in Figs. 7–9. For the outgoing and incoming resonant conditions and in the case of exciton transitions in $In_xGa_{1-x}As$ layers ($x=0.35$), we see a considerable increase in the intensity of the Stokes two-phonon scattering signal (Fig. 7, curve 3). For the $In_xGa_{1-x}As$ layer with nanoislands the outgoing resonant process that can be described by the equation: $E=E_{exc}-K\hbar\omega_{LO}$, where E_{exc} and E are the incident photon energy and exciton energy, respectively, $\hbar\omega_{LO}$ is the phonon energy, and K is the multiphonon order. For the 2D $In_xGa_{1-x}As$ layer with low In content the incoming resonant process is realized ($E=E_{exc}$). In the spectra of resonant Raman scattering, as a rule, the intensity of the one-phonon scattering line is smaller than intensity of the two-phonon scattering line. Therefore, the intense and narrow 2LO-phonon line at 573.6 cm^{-1} (≈ 71.07 meV) with half-width ≈ 10 cm^{-1} is due to scattering in the $In_xGa_{1-x}As$ layer with a lower than $x=0.35$ concentration of In, while the low-frequency broadened 2LO line at ≈ 528 cm^{-1} (≈ 65.46 meV) with half-width ≈ 20 cm^{-1} is due to scattering in the layer enriched with In reaching above $x=0.35$. This data, therefore, are also consistent with a bimodal In distribution.

Generally speaking, when analyzing the Raman spectra of our structures, one should bear in mind that, in addition to signals associated with optical phonons of both the GaAs barrier and the $In_xGa_{1-x}As$ alloy, one must also examine the possible appearance of a discrete set of interface modes IF1, IF2, … localized at the heterostructure boundaries due to the known difference between dielectric constants.[24]

However, previous results[25,26] showed that the IF modes can be neglected for the Raman spectra in Fig. 7, as well as in Figs. 8 and 9, measured under excitation ($E_{exc}=1.165$ eV) far from resonant excitation of GaAs. In particu-

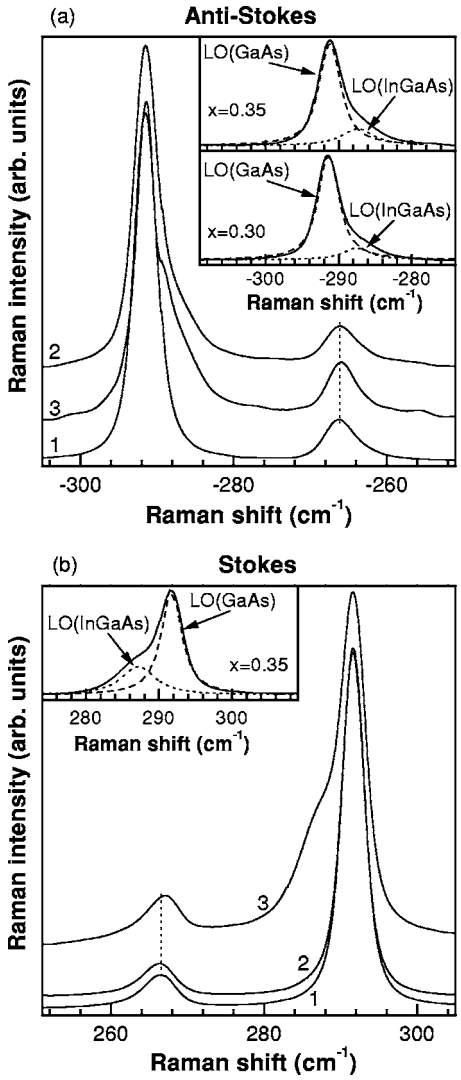

FIG. 8. (a) Anti-Stokes and (b) Stokes Raman spectra of GaAs epilayer (curve 1) and $In_xGa_{1-x}As/GaAs$ multilayer structures with nominal In concentrations of 0.30 and 0.35 (curves 2 and 3, respectively). The spectra are normalized to the intensity of LO (GaAs) line. The insets in (a) and (b) give the Raman spectra of $In_xGa_{1-x}As/GaAs$ multilayer structures in the range of LO phonons and the modeling of these curves by two Lorentz profiles: $E_{exc}=1.165$ eV and $T=300$ K.

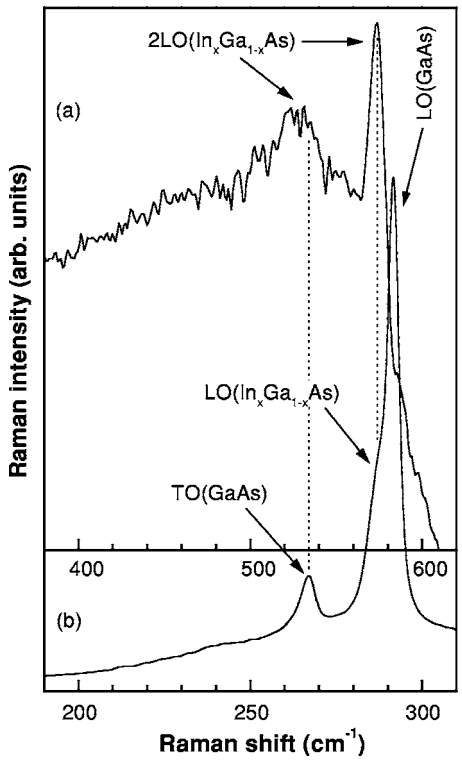

FIG. 9. Resonant Raman spectra of the second order (a) and the first order (b) for the $In_{0.35}Ga_{0.65}As/GaAs$ multilayer structure. The frequency scale of the two-phonon spectrum is reduced by a factor of 2 to plot together with one-phonon spectrum ($E_{exc}=1.165$ eV and $T=300$ K).

lar, the phonon spectra of the first-order scattering in our samples are shown in Fig. 8. Curve 3 in this figure shows that the first-order Stokes spectrum for the sample $x=0.35$. The LO ($In_xGa_{1-x}As$) line can be clearly seen at the low-energy wing of the LO (GaAs)-phonon line of the barrier layers. Modeling these two lines by two Lorentz profiles (see the inset in Fig. 8) enables us to determine the frequency position and half-width of the line due to LO($In_xGa_{1-x}As$) phonons [$\omega_{LO}(In_xGa_{1-x}As)\approx 287$ cm^{-1} and $\Gamma_{LO}(In_xGa_{1-x}As)\approx 5.4$ cm^{-1}]. It is noteworthy that the doubled frequency position of this line corresponds to the frequency of the two-phonon 2LO ($In_xGa_{1-x}As$) line. The latter gives strong evidence that these two LO-phonon lines correspond to scattering from the same layer. The first-order LO ($In_xGa_{1-x}As$)-phonon line (for the sample with $x=0.35$), which corresponds to layers with the lower In concentration, is also seen in the anti-Stokes-scattering spectrum [see the inset in Fig. 8(a)].

Proceeding from the frequency position of the 2LO line of the enriched In sublayer, the respective first-order LO line in the Raman spectrum of InGaAs must be in the near proximity to the TO (GaAs) line. That is why it is not well defined. Its presence is pronounced only in the frequency shift and asymmetry of the bands corresponding to the overlapping of the two lines—TO (GaAs) and LO ($In_xGa_{1-x}As$). However, under resonant conditions of the excitation, is it reliably prominent in the second-order Raman spectrum.

In an InGaAs alloy, optical phonons exhibit a two-mode behavior.[27] That is, both InAs- and GaAs-like modes exist over the whole composition range. In the frequency region of 240 cm^{-1}, we expect LO (InAs)-like modes of $In_xGa_{1-x}As$. But it was difficult for us to reliably observe the InAs LO-like mode. This is explained by the fact that even when In/Ga ratio is close to unity, the intensity of the GaAs LO-like mode dominates in the Raman spectrum.

The data are even more interesting for the sample with $x=0.30$. In this case, although the excitation conditions are identical to the $x=0.35$ case (see the inset in Fig. 7), conditions are more favorable for outgoing resonance of the anti-Stokes LO ($In_xGa_{1-x}As$) phonons. Therefore, it is reasonable to expect a resonant increase in the scattering intensity by LO phonons in the anti-Stokes spectral range, which remarkably was experimentally observed in the sample with $x=0.30$ (Fig. 7, curve 2). The LO ($In_xGa_{1-x}As$)-phonon line from the lower In concentration layers is not pronounced in the Stokes spectral range of the sample, while in the anti-Stokes spectrum it appears again at the low-energy wing of the LO (GaAs)-phonon line of the barrier layers. Thus, the

TABLE III. Frequencies of LO(InGaAs)-like modes for the sample $x=0.35$. $\Delta\omega_{str}^{exp}$ calculated the frequency shifts due to the deformations obtained by HRXRD (Tables I and II). $\Delta\omega_{conf}$ frequency shifts due to confinement Ref. 28. ω_{LO}^{exp} is the experimental value of the frequency for the LO(InGaAs)-like mode. "expt" denotes the experimental data.

x	ω_0^{LO} (GaAs) like (cm^{-1})	$\Delta\omega_{str}^{exp}$ (cm^{-1})	$\Delta\omega_{conf}$ (cm^{-1})	ω_{LO}^{exp} (cm^{-1})
0.65	262.8	2.5	−3	≈264
0.25	282.7	3.4	···	≈287

intensity of the LO ($In_xGa_{1-x}As$)-phonon line depends on the resonant excitation condition and on peculiarities of the resonant amplification for the Stokes-and anti-Stokes-scattering components.

Figure 9 shows the comparison of the Stokes spectra of the first- and second-orders for the sample with $x=0.35$. The frequency scale of the two-phonon spectrum is represented as double. It is seen from the figure that the 2LO ($In_xGa_{1-x}As$)-phonon line corresponds to the low-energy wing of the LO (GaAs)-phonon line. The 2LO (GaAs)-phonon line is absent in the spectrum of the second order, as the excitation conditions are out of resonance in the GaAs layers.

It is important to consider the possibility of the 2LO(GaAs) modes from different GaAs layers. For example, we might question the Raman lines from the protective (capping) and separating (barriers) GaAs layers. However, our analyses of strain values in these layers, which are determined using x-ray measurements [$\varepsilon_{xx}^{spacer}(GaAs)=-5.97\times10^{-4}$, $\varepsilon_{xx}^{cap}(GaAs)=-8.25\times10^{-4}$], show that the possible frequency shift of the LO (GaAs)-phonon line will not exceed 0.2 cm^{-1}.

Generally, it is possible to determine the In content in the QDs and the 2D layer from the measured optical-phonon frequencies. The change in the LO (GaAs)-like-mode frequency for bulk $In_xGa_{1-x}As$ as a function of composition can be described by the relation $\omega(x)=292.3-34.28x-16.92x^2$ with the accuracy of ±0.15 cm^{-1}.[27] However, in our case, the two main effects on the phonon frequencies have to be considered: (1) effects of strain ($\Delta\omega_{str}$) and (2) confinement effects ($\Delta\omega_{conf}$). For the LO modes of $In_xGa_{1-x}As$ layer processes (1) and (2) give opposite frequency shifts. We estimated the low-frequency shift of LO mode caused by $\Delta\omega_{conf}$ according to results of Ref. 28 (see Table III). Effect of strains ($\Delta\omega_{str}$) provides a high-frequency shift of phonon lines, which is a result of compressive strains in the $In_xGa_{1-x}As$ layer due to the lattice mismatch between InGaAs and GaAs, and elastic relaxation because of three-dimensional growth. Therefore, to calculate the phonon frequency shifts due to the strains in the InGaAs layers we used the elastic strains obtained by HRXRD.

In an ideal InGaAs/GaAs heterostructure, $\Delta\omega_{str}$ depends on the strain tensor $\tilde{\varepsilon}_{ij}$ and phonon deformation potential $\tilde{K}_{ij}$. For strained quantum-well (QW) superlattices, the average shear strain components are not taken into consideration, and it is assumed that the barrier material is not strained. The relative frequency shifts for the "singlet" vibration along the [001] [in backscattering geometry from (001) surface, the LO singlet is only Raman active] are given by[25]

$$\frac{\Delta\omega_{str}^{LO}}{\omega_0^{LO}}=\frac{1}{2}\tilde{K}_{11}^{LO}\varepsilon_{zz}+\frac{1}{2}\tilde{K}_{12}^{LO}(\varepsilon_{xx}+\varepsilon_{yy}), \tag{3}$$

where ε_{zz} and $\varepsilon_{xx}=\varepsilon_{yy}$ are the components of the strain tensor related to the lattice mismatch $\varepsilon=(a_{InGaAs}-a_{GaAs})/a_{GaAs}$ and ω_0^{LO} is the frequency of unstrained material. The phonon deformation potentials for $In_xGa_{1-x}As$ were determined using the linear interpolation between binary components of InAs and GaAs: $\tilde{K}_{11}^{LO}(x)=-1.75+0.39\,x$ and $\tilde{K}_{12}^{LO}(x)=-2.45-0.05\,x$.[29]

The values of frequencies of InGaAs LO-like modes for the samples with $x=0.35$ were calculated by means of (3) and are shown in Table III. Obviously, the frequency values for the LO phonons in the Raman spectrum are in good agreement with the calculated ones, considering the values of the strains and layer thicknesses given by HRXRD. Hence, Raman-scattering studies of our multilayer (In,Ga)As/GaAs structures show that each InGaAs layer consists of a thin In-rich sublayer embedded in 2D layer with lower In concentration. These results are in good agreement with the x-ray data.

IV. CONCLUSION

We have reported on investigations of the In distribution in self-assembled, multiple layer $In_xGa_{1-x}As/GaAs$ QD structures. The observation of optical phonons localized in (In,Ga)As QDs and 2D layers using resonant excitation of Raman spectra in the range of the exciton ($e1$-$hh1$) transition is demonstrated. Confined optical phonon frequencies of the QDs and 2D layers measured by means of Raman scattering are in a good agreement with calculated ones, considering the values of the elastic strains and layer thickness given by HRXRD. It is shown that the InGaAs layers in $In_xGa_{1-x}As/GaAs$-stacked QD structures can be effectively modeled as sublayers with two different compositions, i.e., small In-rich regions embedded in a 2D layer having a lower In concentration. This formation is caused by the tendency of the system to reach a thermodynamical equilibrium between the strained $In_xGa_{1-x}As$ layer and the GaAs substrate (separating layers) through a decrease of their lattice parameter mismatch. This process is realized by (i) enriching the intermediate layer with Ga atoms through their migrations from GaAs (intermixing) matrix, and (ii) In surface segregation that results in vacancy generation in the growing layer, which enhances Ga diffusion into these layers.[9–12]

ACKNOWLEDGMENT

The authors acknowledge the financial support of the National Science Foundation of U.S.

[1] *Semiconductor Quantum Dots: Physics, Spectroscopy and Applications*, Nanoscience and Technology, edited by Y. Masumoto and T. Takagahara (Springer-Verlag, Berlin, 2002), p. 486.

[2] K. Mukai, Y. Nakata, K. Otsubo, M. Sugawara, N. Yokoyama, and H. Ishikawa, IEEE J. Quantum Electron. **36**, 472 (2000); F. Heinrichsdorff, Ch. Ribbat, M. Grundmann, and D. Bimberg, Appl. Phys. Lett. **76**, 556 (2000).

[3]T. Lundstrom, W. Shoenfeld, H. Lee, and P. M. Petroff, Science **286**, 312 (1999).
[4]L. Chu, A. Zrenner, G. Böhm, and G. Abstreiter, Appl. Phys. Lett. **76**, 1944 (2000).
[5]J. Y. Yao, T. G. Anderson, and G. L. Dunlop, Semicond. Sci. Technol. **9**, 1086 (1994); V. V. Strelchuk, M. Ya. Valakh, Yu. I. Masur, Z. M. Wang, M. Xiao, and G. J. Salamo, Semiconductors **39**, 127 (2005).
[6]H. Li, Q. Zhuang, Z. Wang, and T. Daniels-Race, J. Appl. Phys. **87**, 188 (2000).
[7]G. G. Tarasov *et al.*, J. Appl. Phys. **88**, 7162 (2000).
[8]Z. M. Wang, K. Holmes, Yu. I. Mazur, and G. J. Salamo, Appl. Phys. Lett. **84**, 1931 (2004).
[9]A. Rosenauer, D. Gerthsen, D. Van Dyck, M. Arzberger, G. Böhm, and G. Abstreiter, Phys. Rev. B **64**, 245334 (2001).
[10]P. B. Jouce, T. J. Krzyzewski, C. G. Bell, B. A. Jouce, and T. S. Jones, Phys. Rev. B **58**, R15981 (1998).
[11]I. Kegel *et al.*, Phys. Rev. B **63**, 035318 (2001).
[12]M. Hanke, D. Grigoriev, M. Schmidbauer, P. Schäfer, R. Köhler, R. L. Sellin, U. W. Pohl, and D. Bimberg, Appl. Phys. Lett. **85**, 3062 (2004).
[13]T. Walther, A. G. Gullis, D. J. Norris, and M. Hopkinson, Phys. Rev. Lett. **86**, 2381 (2001).
[14]M. Schmidbauer, *X-Ray Diffuse Scattering from Self-Organized Mesoscopic Semiconductor Structures*, Springer Tracts in Modern Physics, Vol. 199 (Springer, Berlin, Heidelberg, 2004), p. 204; N. N. Faleev *et al.*, Semiconductors **35**, 932 (2001).
[15]M. A. G. Halliwell, J. Juler, and A. G. Norman, Inst. Phys. Conf. Ser. **67**, 365 (1983).
[16]V. Holy, U. Pietsch, and T. Baumbach, *High-Resolution X-Ray Scattering from Thin Films and Multilayers*, Springer Tracts in Modern Physics, Vol. 149 (Springer, Berlin, Heidelberg, 1999), p. 254.
[17]I. K. Shuller, Phys. Rev. Lett. **44**, 1597 (1980).
[18]C. Priester and M. Lannoo, Phys. Rev. Lett. **75**, 93 (1995).
[19]A. Rosenauer, W. Oberst, D. Litvinov, D. Gerthsen, A. Förster, and R. Schmidt, Phys. Rev. B **61**, 8276 (2000).
[20]N. Peranio, A. Rosenauer, D. Gerthsen, S. V. Sorokin, I. V. Sedova, and S. V. Ivanov, Phys. Rev. B **61**, 16015 (2000).
[21]C. S. Kim *et al.*, Phys. Rev. Lett. **85**, 1124 (2000).
[22]R. Trommer and M. Cardona, Phys. Rev. B **17**, 1865 (1978).
[23]M. Ya. Valakh, V. V. Strelchuk, G. N. Semenova, and Yu. G. Sadofyev, Phys. Solid State **46**, 176 (2004).
[24]P. A. Knipp and T. L. Reinecke, Phys. Rev. B **46**, 10 310 (1992).
[25]*Light Scattering in Solids V: Superlattices and Other Microstructures*, Topics in Applied Physics, Vol. 66, edited by M. Cardona and G. Güntherodt (Springer-Verlag, Berlin, 1989).
[26]Yu. A. Pusep, G. Zanelatto, S. W. da Silva, J. C. Galzerani, P. P. Gonzalez-Borrero, A. I. Toropov, and P. Basmaji, Phys. Rev. B **58**, R1770 (1998).
[27]M. J. L. S. Heines, B. C. Cavenett, and S. T. Davey, Appl. Phys. Lett. **55**, 849 (1989), and references therein.
[28]J. Groenen, A. Mlayah, R. Carles, A. Ponchet, A. Le Corre, and S. Salaün, Appl. Phys. Lett. **69**, 943 (1996).
[29]H. K. Shin, D. J. Lockwood, C. Lacelle, and P. J. Poole, J. Appl. Phys. **88**, 6423 (2000), and references therein.